

Ultrafast proton transfer dynamics of 2-(2'-hydroxyphenyl)benzoxazole dye in different solvents

Simei Sun(孙四梅), Song Zhang(张嵩), Jiao Song(宋娇), Xiaoshan Guo(郭小珊), Chao Jiang(江超), Jingyu Sun(孙静俞), and Saiyu Wang(王赛玉)

Citation: Chin. Phys. B, 2022, 31 (**2**): 027803. DOI: 10.1088/1674-1056/ac3734

Journal homepage: http://cpb.iphy.ac.cn; http://iopscience.iop.org/cpb

What follows is a list of articles you may be interested in

Spectral polarization-encoding of broadband laser pulses by optical rotatory dispersion and its applications in spectral manipulation

Xiaowei Lu(陆小微), Congying Wang(王聪颖), Xuanke Zeng(曾选科), Jiahe Lin(林家和), Yi Cai(蔡懿), Qinggang Lin(林庆钢), Huangcheng Shangguan(上官煌城), Zhenkuan Chen(陈振宽), Shixiang Xu(徐世祥), and Jingzhen Li(李景镇)

Chin. Phys. B, 2021, 30 (**7**): 077801. DOI: 10.1088/1674-1056/abf0fb

Temperature dependent terahertz giant anisotropy and cycloidal spin wave modes in $BiFeO_3$ single crystal

Fan Liu(刘凡), Zuanming Jin(金钻明), Xiumei Liu(刘秀梅), Yuqing Fang(方雨青), Jiajia Guo(国家嘉), Yan Peng(彭滟), Zhenxiang Cheng(程振祥), Guohong Ma(马国宏), Yiming Zhu(朱亦鸣)

Chin. Phys. B, 2020, 29 (**7**): 077804. DOI: 10.1088/1674-1056/ab8dae

Single-shot measurement of THz pulses

Lei Yang(杨磊), Lei Hou(侯磊), Chengang Dong(董陈岗), Wei Shi(施卫)

Chin. Phys. B, 2020, 29 (**5**): 057803. DOI: 10.1088/1674-1056/ab821f

Influence of fluorescence time characteristics on the spatial resolution of CW-stimulated emission depletion microscopy

Haiyun Qin(秦海芸), Wei Zhao(赵伟), Chen Zhang(张琛), Yong Liu(刘勇), Guiren Wang(王归仁), Kaige Wang(王凯歌)

Chin. Phys. B, 2018, 27 (**3**): 037803. DOI: 10.1088/1674-1056/27/3/037803

Photo-induced intramolecular electron transfer and intramolecular vibrational relaxation of rhodamine 6G in DMSO revealed by multiplex transient grating spectroscopy

Jiang Li-Lin, Liu Wei-Long, Song Yun-Fei, Sun Shan-Lin

Chin. Phys. B, 2014, 23 (**10**): 107802. DOI: 10.1088/1674-1056/23/10/107802

Ultrafast proton transfer dynamics of 2-(2′-hydroxyphenyl)benzoxazole dye in different solvents

Simei Sun(孙四梅)[1,†], Song Zhang(张嵩)[2,‡], Jiao Song(宋娇)[1], Xiaoshan Guo(郭小珊)[1], Chao Jiang(江超)[1], Jingyu Sun(孙静俞)[3], and Saiyu Wang(王赛玉)[1]

[1] *Huangshi Key Laboratory of Photoelectric Technology and Materials, College of Physics and Electronic Science, Hubei Normal University, Huangshi* 435002, *China*

[2] *State Key Laboratory of Magnetic Resonance and Atomic and Molecular Physics, Innovation Academy for Precision Measurement Science and Technology, Chinese Academy of Sciences, Wuhan* 430071, *China*

[3] *Hubei Key Laboratory of Pollutant Analysis & Reuse Technology, College of Chemistry and Chemical Engineering, Hubei Normal University, Huangshi* 435002, *China*

(Received 29 July 2021; revised manuscript received 15 October 2021; accepted manuscript online 6 November 2021)

The excited-state intramolecular proton transfer of 2-(2′-hydroxyphenyl)benzoxazole dye in different solvents is investigated using ultrafast femtosecond transient absorption spectroscopy combined with quantum chemical calculations. Conformational conversion from the syn-enol configuration to the keto configuration is proposed as the mechanism of excited-state intramolecular proton transfer. The duration of excited-state intramolecular proton transfer is measured to range from 50 fs to 200 fs in different solvents. This time is strongly dependent on the calculated energy gap between the N-S_0 and T-S_1 structures in the S_1 state. Along the proton transfer reaction coordinate, the vibrational relaxation process on the S_1 state potential surface is observed. The duration of the vibrational relaxation process is determined to be from 8.7 ps to 35 ps dependent on the excess vibrational energy.

Keywords: proton transfer, vibrational relaxation, femtosecond transient absorption spectroscopy, quantum chemical calculations

PACS: 78.47.J–, 82.53.Ps, 82.53.Uv, 87.15.ag **DOI:** 10.1088/1674-1056/ac3734

1. Introduction

As one of the most important and fundamental photoinduced reactions, excited-state intramolecular proton transfer (ESIPT) is a type of photo-tautomerization of a molecule that includes a hydroxyl group, proton donor and a neighboring proton acceptor.[1] Dyes undergoing ESIPT have been applied in many fields,[2–6] for example as fluorescent chemosensors and probes,[7–10] laser dyes,[11,12] UV photostabilizers,[13] promising components for photoswitches[14,15] and organic optoelectronic materials.[16–21] Following photon absorption, ESIPT dyes are widely acknowledged to undergo apparent geometrical reorganization and then present large Stokes shifts. Generally, the ESIPT process derives from the initial S_0 structure (enol) and goes back to the same state through a four-level reaction.[22–26] In this reaction, the excited enol and keto forms in the S_1 state emit short- and long-wavelength fluorescence, respectively.

It is well known that 2-(2′-hydroxyphenyl)benzoxazole (HBO) dye[27,28] and its analog dyes such as 2-(2′-hydroxyphenyl)benzothiazole (HBT)[29,30] and 2-(2′-hydroxyphenyl)benzimidazole (HBI)[31,32] have suitable geometries for ESIPT. The duration of the ESIPT process has been reported as being on the sub-picosecond timescale.[27,28,33–35] Due to the ESIPT effect, HBO and its analog dyes[36,37] have been widely used to produce biological probes and white-light-emitting materials.[4,38–41] Moreover, the introduction of HBO dye into double-stranded DNA can be used to detect a double stranded environment.[42] At present, it is known that HBO dye should be an excellent nonlinear optical material for high-speed and high-sensitivity optical switching devices owing to the ESIPT effect following absorption of the pump pulse rather than a thermal effect.[43]

HBO dye and its derivatives have been widely researched with regard to ESIPT and/or coupled intramolecular charge transfer (ICT).[35,43–49] It was proposed that intramolecular and intermolecular hydrogen bonds contribute to ESIPT and intermolecular proton transfer with solvents, respectively. The timescale of ESIPT was measured by Romesberg and coworkers to be shorter than 170 fs.[38,50] Dynamics simulations of the ESIPT reactions of HBO dye were carried out under the conditions of gas phase and hydration clusters.[35] The results showed that the simulated duration of the ESIPT reaction of HBO dye ranges from 28 fs to 193 fs, and that differences in the duration are due to different initial structures. However, there is still a lack of a direct experimental evidence to confirm the ESIPT time constants simulated in gas and hydrated clusters. On the other hand, dual emission of HBO dye is not shown in all solvents. The long-wavelength emission has consistently been considered as the fluorescence from the S_1 state of the keto tautomer[38,50–52] and, although contentious, the

†Corresponding author. E-mail: simeisun@hbnu.edu.cn
‡Corresponding author. E-mail: zhangsong@wipm.ac.cn

© 2022 Chinese Physical Society and IOP Publishing Ltd

short-wavelength emission is considered as fluorescence from the S_1 state of the anti-enol form or syn-enol form. Moreover, although the differences in the lifetimes of the S_1 state of the keto tautomer in different solvents are often discussed the differences in ESIPT dynamics and their causes have not been discussed in detail.

In this work, ultrafast femtosecond transient absorption (fs-TA) spectroscopy technology and global fitting were employed to clarify the ESIPT process and the following ultrafast radiative and nonradiative dynamics of HBO dye in cyclohexane, 1,4-dioxane and ethanol. Moreover, quantum chemical (QC) calculations were performed to analyze the excited state dynamics. Three fs-TA spectral bands and three lifetimes were obtained in the fs-TA experiments. The QC calculations were carried out to explain the dynamics of ESIPT and vibrational relaxation (VR). Based on the novel experimental and theoretical results, dual emission of short and long fluorescence was clearly assigned, and a more detailed ESIPT diagram is provided.

2. Experimental and theoretical methods

2.1. Experimental method

HBO dye and solvents (cyclohexane, 1,4-dioxane and ethanol) were purchased from Sigma. With purity higher than 99%, both the solute and solvents were used without further purification. All measurements were performed at room temperature and fresh samples were used for each measurement. The concentration of HBO dye in solvents was set as 1 mM.

A UV-vis spectrometer (INESA, L6) was used to record the steady absorption spectra in a 1 cm quartz cell and a spectrometer (Princeton, SpectraPro 2500i) was used to record the fluorescence spectra in a 1 mm quartz cell. The setup to record the fs-TA spectra was based on the Ti:sapphire femtosecond laser system and has been described in detail in previous works.[53,54] Briefly, the seed beam of the femtosecond laser was generated by a commercial Ti:sapphire oscillator and then amplified to output a fundamental pulse (1 kHz, 1 mJ, 35 fs and 800 nm). The 800 nm femtosecond pulse was divided into two beams. One beam with energy of about 4 μJ was focused on a 1 mm CaF_2 plate to generate a broad-band continuum to obtain signal and reference beams as a probe pulse. The other beam had a higher intensity and was sent to a home-built non-collinear optical parametric amplifier (NOPA) system to generate a pump pulse at a wavelength of 344 nm. A small part of the second beam was also split to generate continuum for the signal of the NOPA system. A 400 nm femtosecond pulse was generated by a beta barium borate (BBO) crystal through second-harmonic generation of the 800 nm femtosecond pulse and used to amplify the signal pulse at the desired 660 nm pulse. An excitation pulse with a wavelength of 344 nm, the energy of which was about 0.6 μJ at the sample position, represented the harmonic generation of the 800 nm and 660 nm pulses by the BBO crystal. The NOPA pulses were temporally compressed to give the minimum pulse width, which was completed by prism gratings. The geometry and polarization between the excitation and signal pulses were set as $\sim 4^\circ$ and the magic angle, respectively, with the reference beam transmitting through the sample at a different spot. The delay time between the probe and pump beam was realized and monitored by a linear translation stage. A spectrometer (Princeton, SpectraPro 2500i), equipped with a CCD camera (PI-MAX, 1024×256 pixel array) was used to detect the fs-TA spectra. The optical Kerr gate method was used to measure the instrumental response function, which is typically better than 100 fs at wavelengths shorter than 500 nm, and a little longer at a wavelength of 650 nm.

2.2. Theoretical method

All QC calculations were carried out using the Gaussian16W.[55] PBE1PBE method with a 6-311G(d,p) basis set was used to optimize the geometries of the S_0 and S_1 states of HBO dye in the gas phase, cyclohexane, ethanol and 1,4-dioxane. Vibrational frequencies were analyzed to confirm the stationary points. The energies of the ground and excited states were calculated using the PBE1PBE function at the optimized structures of the S_0 and S_1 states. The Boltzmann distribution of different configurations in the S_0 state was also found according to the energy of the S_0 state of different configurations using the program Molclus.[56] Using the polarizable continuum model with the integral equation formalism, a self-consistent reaction field was used to consider the effect of the bulk solvent dielectric, which is expected to affect the geometries and energies of the ground and excited states.

3. Results and discussion

3.1. Configurations in the S_0 and S_1 states

As shown in Fig. 1, the S_0 state geometry of HBO dye was optimized in the gas phase and three solvents, starting with enol and keto structures and ending only with enol forms, where the enol forms have local minima and no virtual frequencies. In the S_0 state, there are four enol configurations of HBO dye: 1, syn-enol; 2, anti-enol; 3, anti-enol open; 4, syn-enol open (shown in Fig. 1(a)). The calculated energies and Boltzmann distribution of the four configurations in gas and solvents in the S_0 state are listed in Table 1. The results show that the normal syn-enol form, denoted as the N-S_0 structure, has the lowest energy. The normal syn-enol form in the S_0 state is most stable, the population of which is dominant whether it is in the gas phase or solvents. Compared with the Boltzmann distribution in the gas phase, cyclohexane and 1,4-dioxane, the distribution in ethanol is different. The results show the proportion of anti-enol form is not zero but still very small, indicating that the anti-enol open structure may exist but its probability is very small.

Table 1. The energy difference ΔE related to the energy of the most stable configuration and the Boltzmann distribution of different configurations of HBO dye in the ground state in gas and different solvents at room temperature.

Configuration	Gas		Cyclohexane		1,4-dioxane		Ethanol	
	ΔE (kcal/mol)	Boltzmann distribution (%)	ΔE (kcal/mol)	Boltzmann distribution (%)	ΔE (kcal/mol)	Boltzmann distribution (%)	ΔE (kcal/mol)	Boltzmann distribution (%)
Syn-enol	0.00	100.00	0.00	100.00	0.00	100.00	0.00	99.99
Anti-enol	6.52	0.00	6.19	0.00	6.52	0.00	5.67	0.01
Anti-enol open	11.76	0.00	10.48	0.00	10.81	0.00	8.73	0.00
Syn-enol open	12.62	0.00	11.11	0.00	11.47	0.00	8.90	0.00

Optimization of S_1 state geometry was also performed on syn-enol and keto structures in the gas phase and solvents. The symbols N-S_1 and T-S_1 are used to refer to the optimized S_1 state structure of syn-enol and keto forms (shown in Fig. 1(b)), respectively. The energy of the S_1 state of the T-S_1 structure is slightly lower than that of the N-S_1 structure, as listed in Table 2. This indicates that the keto tautomer is more stable than the syn-enol form in the S_1 state. Since the keto tautomer of HBO dye in the S_0 state has no local minima, it is unstable and can easily return to the normal syn-enol form in the S_0 state.[38,43,47] In Table 2, ΔE_1 and ΔE_2 represent the energy gaps of the N-S_0 and N-S_1 structures, respectively, compared with that of the T-S_1 structure in the S_1 state. It is found that ΔE_1 and ΔE_2 possibly stand for the ability for the ESIPT process and excess vibrational energy, respectively.

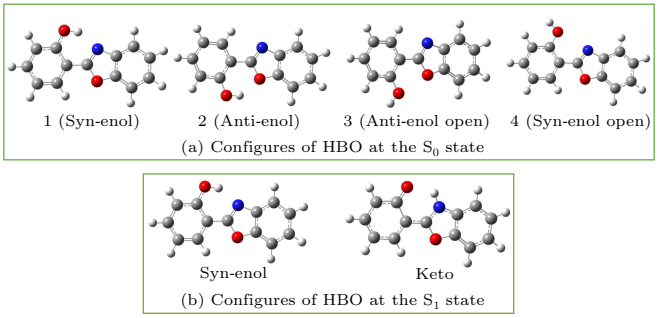


Fig. 1. Optimized configurations of HBO dye in the gas phase in the S_0 state (a) and the S_1 state (b).

For convenience, only the frontier molecular orbits were calculated in the gas phase. Figure 2 shows three molecular orbits of the N-S_0 and the T-S_1 structures. Calculated results show that the S_1 state of the N-S_0 structure has a large transition strength and is dominated by the 56 $\leftarrow$ 55 transition with an energy of 4.0342 eV. The S_2 state of the N-S_0 structure mainly corresponds to the 56 $\leftarrow$ 54 transition, the transition strength of which is much weaker than that of the S_1 state. The 55 and 56 orbits belong to π and π^* orbits and correspond to the highest occupied molecular orbital (HOMO) and lowest unoccupied molecular orbital (LUMO), respectively. Consequently, it is determined that the excitation to the S_1 state of the N-S_0 structure is strongly allowed with the dominant transition from HOMO to LUMO, while the excitation to the S_2 state is weaker with the transition from HOMO-1 to LUMO. The frontier molecular orbits of the N-S_1 structure were also calculated in the same way as that of the N-S_0 structure. The results are similar to that of the N-S_0 structure. As shown in Fig. 2, due to the structural reorganization, the molecular orbits of the T-S_1 structure are quite different from those of N-S_0 structure.

Table 2. The vertical energies (eV) of the S_0 and S_1 states of the N-S_0, N-S_1, and T-S_1 structures of HBO dye in gas and different solvents. $\Delta E_1 = S_1(\text{N-}S_0) - S_1(\text{N-}S_1)$, $\Delta E_2 = S_1(\text{N-}S_1) - S_1(\text{T-}S_1)$.

Solvent		Structure			ΔE_1	ΔE_2
		N-S_0	N-S_1	T-S_1		
Gas	S_0 state	0.0000	0.2173	0.8817		
	S_1 state	4.0342	3.8314	3.6537	0.3805	0.1777
Cyclohexane	S_0 state	0.0000	0.2057	0.7908		
	S_1 state	3.9709	3.7658	3.5844	0.3865	0.1814
Ethanol	S_0 state	0.0000	0.2618	0.6657		
	S_1 state	4.0187	3.6351	3.4566	0.5621	0.1785
1,4-gioxane	S_0 state	0.0000	0.2095	0.7786		
	S_1 state	3.9822	3.7571	3.5758	0.4064	0.1814

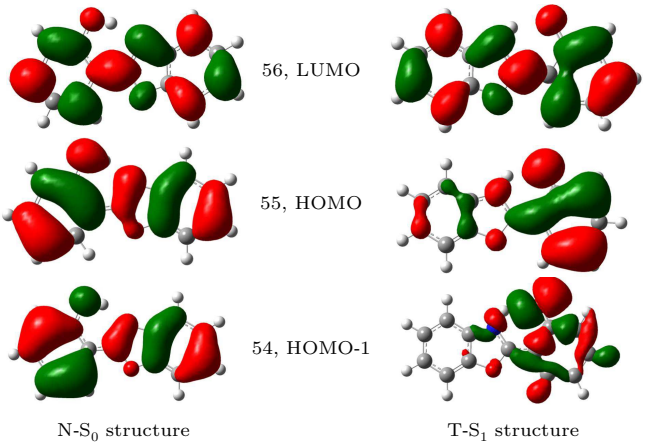


Fig. 2. Frontier orbitals in the gas phase: HOMO-1, HOMO and LUMO of HBO dye at equilibrium geometries of the N-S_0 (left) and T-S_1 (right) structures. Calculations were performed based on the PBE1PBE method with the 6-311G(d,p) basis set.

3.2. The assignment of long- and short-wavelength fluorescence

Figure 3 depicts the steady absorption and fluorescence spectra of HBO dye in cyclohexane, 1,4-dioxane and ethanol. At wavelengths longer than 300 nm there are two absorption peaks which are a small blue shift with the increasing polarity of the solvents. The peaks at 332 nm and 320 nm were assigned to the syn-enol and anti-enol open tautomer of HBO

dye, respectively.[38,40] The Boltzmann distribution of different configurations of HBO dye in the S_0 state shows that the proportion of syn-enol form in the gas phase and three solvents is almost 100%, which indicates that the syn-enol form is absolutely dominant. So, the 320 nm peak could not be assigned to the absorption of the anti-enol open form. It may be due to higher excited states or the S_1 state with higher vibrational energies.

The steady fluorescence spectra of HBO dye in cyclohexane and 1,4-dioxane show a strong and broad band around 510 nm. This long-wavelength fluorescence band with a large Stokes shift can be consistently assigned to the emission from the excited keto form transferred from the excited syn-enol.[50–52] The long-wavelength fluorescence, with strong intensity and large Stokes shift, proves an easy and effective process for ESIPT. The long-wavelength fluorescence of HBO dye in ethanol is blue shifted to 495 nm compared with that in 1,4-dioxane and cyclohexane. Furthermore, the short-wavelength band around 390 nm in ethanol is much weaker than the long-wavelength band, and was previously assigned to the emission from the excited syn-enol tautomer or excited anti-enol open tautomer.[38,43,50]

However, the excitation wavelength of 344 nm used in this experiment is located at the absorption edge of the syn-enol form. It is indicated that the syn-enol form of HBO dye is most easily excited here. Consequently, we assign the short-wavelength fluorescence to the emission from the S_1 state of the syn-enol form. This viewpoint is also supported by the phenomenon in the fs-TA spectra in which the decay of the short-wavelength stimulated emission (SE) signal is distributed to the rise of the long-wavelength SE signal.

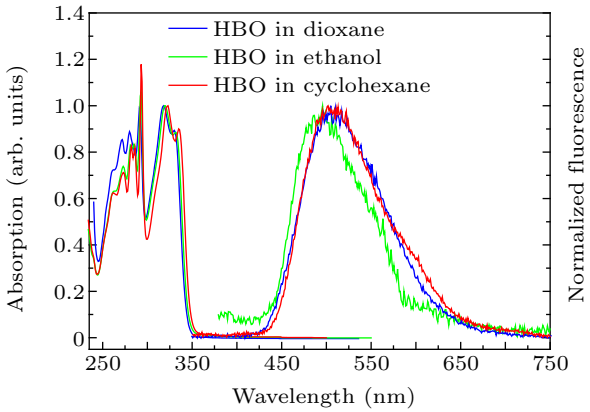


Fig. 3. Steady absorption and fluorescence spectra of HBO dye in 1,4-dioxane (blue), ethanol (green) and cyclohexane (red). Fluorescence spectra were measured upon excitation at 344 nm.

3.3. The ESIPT dynamics

The fs-TA spectra of HBO dye at delay times within 30 ps and 500 ps are shown in Figs. 4(a) and 4(b), respectively. The fs-TA spectra were recorded from 380 nm to 750 nm upon excitation at 344 nm, and three broad bands were observed. The red, first band of positive signal with wavelength shorter than 450 nm is attributed to excited state absorption (ESA1). The blue, second band of negative signal from 450 nm to 620 nm is from SE. The red, third band of positive signal with wavelength longer than 620 nm is assigned to ESA2. Obviously, all the three bands are completely attenuated to zero within 500 ps.

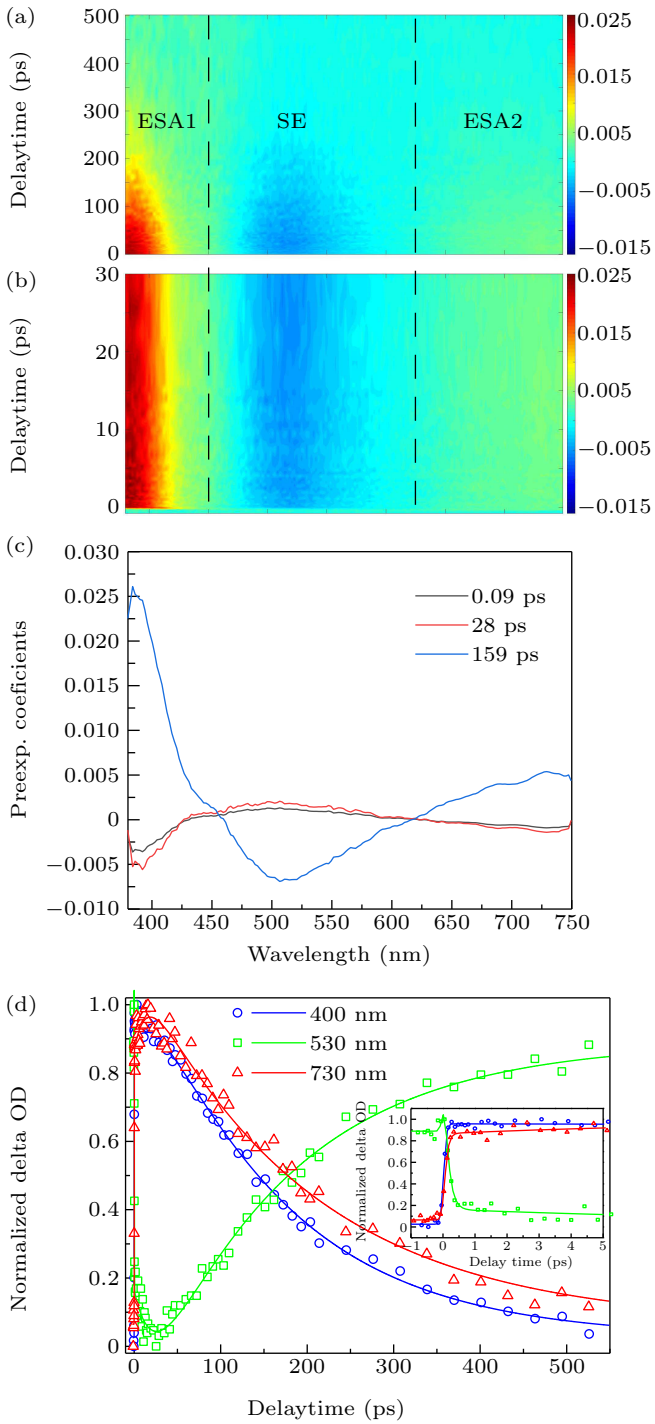


Fig. 4. Broad fs-TA spectra of HBO dye in 1,4-dioxane at 0 ps–500 ps (a) and 0 ps–30 ps (b). The decay-associated difference spectra (DADS) and the corresponding lifetime (c) and the time profiles at the selected wavelengths (d).

In order to accurately analyze the dynamics of HBO dye observed in the fs-TA spectra in 1,4-dioxane, singular value decomposition analysis and global fitting were performed on

the two-dimensional data matrix, which outputs three DADS components with lifetimes of 90 fs (τ_1), 28 ps (τ_2) and 159 ps (τ_3), shown in Fig. 4(c). The longitudinal coordinates of DADS are the pre-exponential factors of the related lifetime components and present the relative contribution at each wavelength. There is more than one spectral component at some wavelengths since the signals originating from different states overlap at some wavelengths.

The temporal behavior of the ESA1, SE and ESA2 signals is described by the decay of typical wavelengths of 400 nm, 530 nm, and 730 nm, respectively. In Fig. 4(d), the fitted decay curves match well with the experimental traces, indicating that the results of global analysis are credible. The fs-TA spectra, DADS spectra and time profiles of HBO dye in ethanol and cyclohexane are shown in Figs. S1 and S2, respectively. The global fitted time constants of HBO in three solvents, as well as the polarity and viscosity of solvents, are list in Table 3.

Table 3. The polarity, viscosity and time constants of HBO dye in cyclohexane, ethanol and 1,4-dioxane.

Solvent	Polarity	Viscosity	τ_1 (ps)	τ_2 (ps)	τ_3 (ps)
Cyclohexane	0.1	1.0	0.20 ± 0.02	35 ± 6	265 ± 10
Ethanol	4.3	1.2	0.05 ± 0.01	8.7 ± 4	128 ± 8
1,4-dioxane	4.8	1.5	0.09 ± 0.01	28 ± 4	159 ± 8

The long-wavelength emission with strong intensity and broad bandwidth of the keto tautomer reasonably indicates that it is easy to experience the ESIPT process — from the syn-enol form to the keto tautomer in the S_1 state (Fig. 5).[38,43,50] The 159 ps blue component of DADS, shown in Fig. 4(c), is dominant, including positive signals of wavelengths shorter than 450 nm or longer than 620 nm, and negative signals of wavelengths between 450 nm and 620 nm. The three areas correspond to ESA1, SE and ESA2 bands of the broad fs-TA spectra of HBO dye in 1,4-dioxane, shown in Figs. 4(a) and 4(b), respectively. Since the peak of the SE band is in accordance with the steady fluorescence, it is indicated that the component of several hundreds ps derives from the S_1 state of the keto tautomer.[50] The ESA1 and ESA2 bands could be assigned to the $S_1 \rightarrow S_m$ and $S_1 \rightarrow S_n$ absorption of the keto tautomer.

In Figs. S1 and S2, the delay times of 128 ps and 265 ps are assigned to the S_1 state lifetimes of the keto tautomer in ethanol and cyclohexane, respectively. Glasbeek concluded that the S_1 state lifetime of the keto form decreases with decreasing solvent viscosity and increasing solvent polarity.[50] In this work, the S_1 state lifetime of the keto tautomer of HBO dye was measured to be from 128 ps to 265 ps in different solvents. It is seen that the lifetime of the keto tautomer shows an obvious contrary trend to the solvent polarity, which is in accordance with the results of time-resolved fluorescence[38] and femtosecond fluorescence upconversion.[50] However, it is a little unusual that the lifetime of the keto tautomer in 1,4-dioxane is somehow longer than that in ethanol. This is possibly due to the intermolecular hydrogen-bond interaction between ethanol and N or O atoms of HBO.[48] Moreover, we did not observe the phenomenon that the S_1 state lifetime of the keto tautomer decreases with decreasing solvent viscosity.

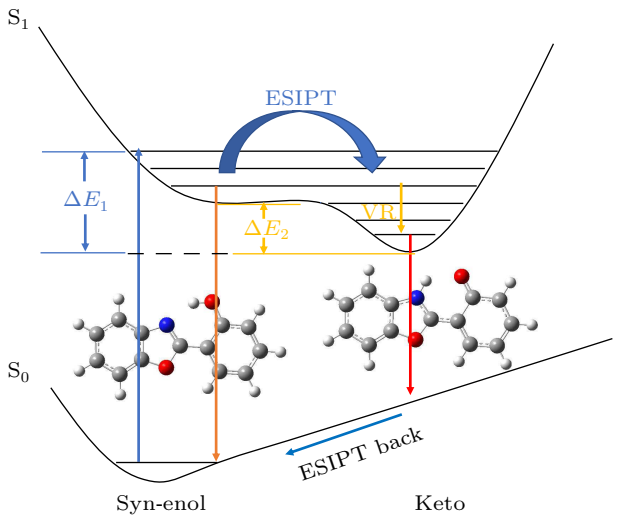


Fig. 5. Schematic diagram of the ESIPT dynamics of HBO dye. The Franck–Condon excitation is presented by the blue arrow. The short-wavelength emission from the syn-enol form is confirmed and is very weak because of the barrierless ESIPT process. The VR process existing in the S_1 state potential and the long-wavelength emission from the keto tautomer is strong for the ultrafast ESIPT process. Because of the unstable structure, the keto form returns to the syn-enol form easily in the S_0 state.

As listed in Table 2, the energy of the T-S_1 structure in the S_1 state is about 0.2 eV lower than that of the N-S_1 structure and the duration of ESITP process is on the femtosecond scale. This theoretically and experimentally illustrates a barrierless S_1 potential and an ultrafast ESIPT process of HBO. The barrierless ESIPT process promotes the keto fluorescence and quenches the enol fluorescence. This is supported by the fact that no obvious or strong short-wavelength steady fluorescence can be observed in the three solvents. The 90 fs black component of DADS has a remarkable negative signal before 420 nm. This short-wavelength SE band is not obviously shown in Fig. 4(a) because it is overlapped and submerged into the ESA1 band. The pre-exponential factor of the black component is contrary to that of the blue component, indicating that the attenuation of the short-wavelength SE band contributes to the appearance of the long-wavelength SE band. This shows that the decay of the state assigned to the black component results in a rise of the state assigned to the blue component. Consequently, the black component could be assigned to the S_1 state of the syn-enol configuration, and the duration of 90 fs should be assigned to the ESIPT process, which was inferred as 170 fs owing to the limit of the instrumental response function.[50]

The 0.05 ps and 0.20 ps components are assigned to the ESIPT process in ethanol and cyclohexane, respectively. The ESIPT time in 1,4-dioxane and ethanol is obviously shorter than that in cyclohexane. The energy gap ΔE_1 between the N-S_0 and T-S_1 structures in the S_1 state in cyclohexane, ethanol

and 1,4-dioxane is 0.3865 eV, 0.5621 eV, and 0.4064 eV, respectively, and the corresponding ESIPT time is 0.20 ps, 0.05 ps, and 0.09 ps, respectively. It is concluded that the duration of the ESIPT process decreases with increasing energy gap ΔE_1. The higher the energy gap ΔE_1, the steeper the potential energy surface of the S_1 state. The steepness indicates the ease of the ESIPT process, wherein ethanol solvent environment provides a higher ΔE_1 to promote a faster ESIPT process.

3.4. VR process

According to the timescales of the red component in Fig. 4 and Figs. S1, S2, the corresponding process could be assigned to the VR process,[38,50] shown in Fig. 5. The behavior of the red DADS spectra is different in the three solvents. The pre-exponential factor of the red DADS spectrum in 1,4-dioxane is opposite to that of the blue DADS spectrum, while the pre-exponential factor of the red DADS spectrum in cyclohexane is synonymous to that of the blue DADS spectrum and that in ethanol is much more complex and irregular. These phenomena show a complicated VR process.

The energy gap ΔE_2 between the N-S_1 and T-S_1 structures in the S_1 state may represent the excess vibrational energy on the S_1 state potential. The excess vibrational energy could dissipate by intramolecular or intermolecular interactions. The more greater the excess vibrational energy, the longer the time needed for the VR process. In ethanol, the excess vibrational energy is 0.1785 eV and the duration of the VR process is 8.7 ps, whereas the excess vibrational energy in both 1,4-dioxane and cyclohexane is 0.1814 eV and the duration of the VR process is lengthened to 28 ps and 35 ps, respectively. Compared with timescale of VR in cyclohexane and 1,4-dioxane, that in ethanol is significantly reduced. Consequently, in ethanol, the VR process not only occurs in intramolecular systems but also may occur in intermolecular systems. Intermolecular interaction may due to the interaction between solvents and the N or O atoms of HBO. Moreover, according to the Einstein formula, the theorical lifetime of the S_1 state of the keto form can be calculated as $\tau = 1.5/(f \times \Delta E^2)$. The $S_1 \leftarrow S_0$ vertical transition energy/strength of the T-S_1 structure is 2.7945 eV/22539.7 cm^{-1} and 0.3172 in ethanol, giving a keto lifetime 6.31 ns. The theorical lifetime is much longer than the experimental data of 128 ps. This indicates that there may exist some nonradiative processes such as internal conversion and external conversion.

4. Conclusion

The ESIPT dynamics of HBO dye in three solvents were investigated by ultrafast experiments combined with theoretical calculations. The calculated results show that only four enol configurations exist in the S_0 state, and the Boltzmann distribution shows that the syn-enol form is absolutely dominant. In the S_1 state, however, enol and keto forms are obtained and the dominant keto fluorescence shows an easy ESIPT process. The ESIPT process occurs within 50 fs–200 fs and strongly depends on the energy gap ΔE_1 between the N-S_0 and T-S_1 structures in the S_1 state. The VR process has also been observed and takes 8.7 ps–35 ps in different solvents. The VR process is obviously dependent on the excess vibrational energy ΔE_2. The S_1 state lifetime of the keto form following the ESIPT process depends on the polarity of the solvent. This work yields a physical principal and clear mechanism for the photoinduced ESIPT dynamics in HBO dye, and provides theoretical guidance for the design and implementation of optical switching devices.

Acknowledgments

Project supported by the Natural Science Foundation of Hubei Province, China (Grant No. 2020CFB468), the Guiding Project of Scientific Research Plan of Department of Education of Hubei Province, China (Grant No. B2020136), and the National Key Research and Development Program of China (Grant No. 2019YFA0307700), and the National Natural Science Foundation of China (Grant Nos. 11974381, 11674355, and 21507027).

References

[1] Formosinho S J and Arnaut L G 1993 *J. Photoch. Photobio. A* **75** 21
[2] Chen W, Wright B D and Pang Y 2012 *Chem. Commun.* **48** 3824
[3] Patil V S, Padalkar V S, Tathe A B and Sekar N 2013 *Dyes Pigm.* **98** 507
[4] Kim S, Seo J, Jung H K, Kim J J and Park S Y 2005 *Adv. Mater.* **17** 2077
[5] Park S, Kim S, Seo J and Park S Y 2008 *Macromol. Res.* **16** 385
[6] Park S, Seo J, Kim S H and Park S Y 2008 *Adv. Funct. Mater.* **18** 726
[7] Wu J, Liu W, Ge J, Zhang H and Wang P 2011 *Chem. Soc. Rev.* **40** 3483
[8] Zhao J, Ji S, Chen Y, Guo H and Yang P 2012 *Phys. Chem. Chem. Phys.* **14** 8803
[9] Rodembusch F S, Leusin F P, da Costa Medina L F, Brandelli A and Stefani V 2005 *Photoch. Photobio. Sci.* **4** 254
[10] Abou-Zied O K 2012 *Phys. Chem. Chem. Phys.* **14** 2832
[11] Sastre R and Costela A 1995 *Adv. Mater.* **7** 198
[12] Costela A, Garcia-Moreno I, Figuera J M, Amat-Guerri F and Sastre R 1996 *Appl. Phys. Lett.* **68** 593
[13] Fluegge A P, Waiblinger F, Stein M, Keck J, Kramer H E A, Fischer P, Wood M G, DeBellis A D, Ravichandran R and Leppard D 2007 *J. Phys. Chem. A* **111** 9733
[14] Lim S J, Seo J and Park S Y 2006 *J. Am. Chem. Soc.* **128** 14542
[15] Mutai T, Tomoda H, Ohkawa T, Yabe Y and Araki K 2008 *Angew. Chem. Int. Ed. Engl.* **47** 9522
[16] You Y, Seo J, Kim S H, Kim K S, Ahn T K, Kim D and Park S Y 2008 *Inorg. Chem.* **47** 1476
[17] Park S, Kwon J E, Kim S H, Seo J, Chung K, Park S Y, Jang D J, Medina B M, Gierschner J and Park S Y 2009 *J. Am. Chem. Soc.* **131** 14043
[18] Zhao J, Chen J, Liu J and Hoffmann M R 2015 *Phys. Chem. Chem. Phys.* **17** 11990
[19] Zhao J, Dong H and Zheng Y 2018 *J. Lumin.* **195** 228
[20] Štacko P, Kistemaker J C M, van Leeuwen T, Chang M C, Otten E and Feringa B L 2017 *Science* **356** 964
[21] Ríos Vázquez S, Ríos Rodríguez M C, Mosquera M and Rodríguez-Prieto F 2007 *J. Phys. Chem. A* **111** 1814
[22] Duarte L, Germino J C, Braga C A, Barboza C A, Atvars T D Z, Santos F D S and Rodembusch F S 2018 *Photoch. Photobio. Sci.* **17** 231

[23] Liu Y H, Wang S M, Zhu C and Lin S H 2017 *New J. Chem.* **41** 8437
[24] Yang D, Zhao J, Yang G, Song N, Zheng R and Wang Y 2017 *J. Mol. Liq.* **241** 1003
[25] Zhao J, Dong H and Zheng Y 2018 *J. Phys. Chem. A* **122** 1200
[26] Yang D, Zhao J, Yang G, Song N, Zheng R and Wang Y 2017 *Org. Chem. Front.* **4** 1935
[27] Krishnamurthy M and Dogra S K 1986 *J. Photochem.* **32** 235
[28] Chen W H and Pang Y 2010 *Tetrahedron Lett.* **51** 1914
[29] Barbatti M, Aquino A J, Lischka H, Schriever C, Lochbrunner S and Riedle E 2009 *Phys. Chem. Chem. Phys.* **11** 1406
[30] Kungwan N, Plasser F, Aquino A J, Barbatti M, Wolschann P and Lischka H 2012 *Phys. Chem. Chem. Phys.* **14** 9016
[31] Walter J L and Freiser H 1953 *Anal. Chem.* **25** 127
[32] Roberts E L, Dey J and Warner I M 1997 *J. Phys. Chem. A* **101** 5296
[33] Ohshima A, Momotake A, Nagahata R and Arai T 2005 *J. Phys. Chem. A* **109** 9731
[34] Abou-Zied O K 2007 *Chem. Phys.* **337** 1
[35] Daengngern R and Kungwan N 2014 *Chem. Phys. Lett.* **609** 147
[36] Ormson S M and Brown R G 1994 *Prog. React. Kinet.* **19** 45
[37] Ríos Vázquez S, Ríos Rodríguez M C, Mosquera M and Rodríguez-Prieto F 2008 *J. Phys. Chem. A* **112** 376
[38] Abou-Zied O K, Jimenez R, Thompson E H Z, Millar D P and Romesberg F E 2002 *J. Phys. Chem. A* **106** 3665
[39] Zhong D, Douhal A and Zewail A H 2000 *Proc. Natl. Acad. Sci. USA* **97** 14056
[40] Taki M, Wolford J L and O'Halloran T V 2004 *J. Am. Chem. Soc.* **126** 712
[41] Padalkar V S, Ramasami P and Sekar N 2014 *J. Lumin.* **146** 527
[42] Ogawa A K, Abou-Zied O K, Tsui V, Jimenez R, Case D A and Romesberg F E 2000 *J. Am. Chem. Soc.* **122** 9917
[43] Zhang G, Wang H, Yu Y, Xiong F, Tang G and Chen W 2003 *Appl. Phys. B* **76** 677
[44] Alarcos N, Gutierrez M, Liras M, Sanchez F, Moreno M and Douhal A 2015 *Phys. Chem. Chem. Phys.* **17** 14569
[45] Alarcos N, Gutierrez M, Liras M, Sanchez F and Douhal A 2015 *Phys. Chem. Chem. Phys.* **17** 16257
[46] Lu X, Zhai Y, Song P and Zhang M 2018 *Struct. Chem.* **29** 1655
[47] Kim C H, Park J, Seo J, Park S Y and Joo T 2010 *J. Phys. Chem. A* **114** 5618
[48] Azarias C, Budzak S, Laurent A D, Ulrich G and Jacquemin D 2016 *Chem. Sci.* **7** 3763
[49] Alarcos N, Gutierrez M, Liras M, Sanchez F and Douhal A 2015 *Photoch. Photobio. Sci.* **14** 1306
[50] Wang H, Zhang H, Abou-Zied O K, Yu C, Romesberg F E and Glasbeek M 2003 *Chem. Phys. Lett.* **367** 599
[51] Corbellini V A, Scroferneker M L, Carissimi M, Rodembusch F S and Stefani V 2010 *J. Photoch. Photobio. B* **99** 126
[52] Rodembusch F S, Leusin F P, Campo L F and Stefani V 2007 *J. Lumin.* **126** 728
[53] Zhang S, Sun S, Zhou M, Wang L and Zhang B 2017 *Sci. Rep.* **7** 43419
[54] Sun S, Qin C, Liu H and Jiang C 2020 *Spectrochim. Acta A* **234** 118200
[55] Frisch M J, Trucks G W, Schlegel H B, *et al.* 2016 *Gaussian 16*, Revision A.03, Gaussian, Inc., Wallingford CT.
[56] Tian L 2019 *Molclus program*, Version 1.8.9 (accessed 2019-Sep-28)